

Article

Porous and Dense Alginate/Chitosan Composite Films Loaded with Simvastatin for Dressing Applications

Rubens T. Monteiro ¹, Thamyres F. Da Silva ¹, Luciana de Souza Guedes ¹, Raimundo N. F. Moreira Filho ¹, Ana L. B. Soares ¹, Niédja F. Vasconcelos ², Fabia K. Andrade ¹ and Rodrigo S. Vieira ^{1,*}

¹ Department of Chemical Engineering, Federal University of Ceará, Fortaleza 60455-760, Brazil; rubens.engenheiroquimico@gmail.com (R.T.M.); thamyres.freire@hotmail.com (T.F.D.S.); lsouguedes@hotmail.com (L.d.S.G.); nonatofernandes@alu.ufc.br (R.N.F.M.F.); analorenasoaes@gmail.com (A.L.B.S.); fabiakarine@gmail.com (F.K.A.)

² Centro de Tecnologias Estratégicas do Nordeste (CETENE), Recife 50740-545, Brazil; niedjafittipaldi@hotmail.com

* Correspondence: rodrigo@gpsa.ufc.br; Tel.: +55-85-98696-2919

Abstract: Alginate is a biocompatible polysaccharide matrix used for bioactive dressings with inherent healing properties. Most alginate dressings are produced as single-layer dressings. This study explores the potential of bilayer membranes to modulate drug release and enhance antimicrobial properties. We used alginate and chitosan loaded with simvastatin, an anti-inflammatory drug. One membrane comprised dense layers of both alginate and chitosan, while the other featured a dense alginate upper layer and a porous chitosan lower layer. The current study introduces a new approach in which a bilayer membrane is modeled instead of creating a polymeric blend between alginate and chitosan. The upper layer of the membrane contains only alginate loaded with simvastatin, while the bottom layer contains only chitosan. Another innovation is the study of the use of a porous lower layer of chitosan. Therefore, the association of these polymers in a bilayer and porous membrane gives advanced therapeutic dressings (with anti-inflammatory and antimicrobial properties intrinsic to the membrane) that are more efficient in the healing of complex wounds. Comprehensive characterization encompassed physicochemical, thermal, morphological, and mechanical properties. Microbiological tests were conducted using chitosan extract, and cytotoxicity evaluations were performed on fibroblast and keratinocyte cells. The results showed interlayer adhesion due to ionic interactions between alginate and chitosan surfaces. The drying process influenced the morphological and physicochemical features of the membranes. Simvastatin release profiles demonstrated sustained release over an extended period (approximately 60%–70% of the drug after 96 h). Storage assessments revealed that after six months, the membranes maintained around 98% of the initial simvastatin content. The antimicrobial activity test underscored the bacteriostatic efficacy of the chitosan porous layer, making it well-suited for infected wounds. Cell viability tests confirmed the non-cytotoxic nature of the films, highlighting their promising characteristics for treating diverse skin lesion types.

Keywords: alginate; chitosan; dressings; simvastatin; controlled drug release



Citation: Monteiro, R.T.; Da Silva, T.F.; de Souza Guedes, L.; Moreira Filho, R.N.F.; Soares, A.L.B.; Vasconcelos, N.F.; Andrade, F.K.; Vieira, R.S. Porous and Dense Alginate/Chitosan Composite Films Loaded with Simvastatin for Dressing Applications. *Coatings* **2024**, *14*, 278. <https://doi.org/10.3390/coatings14030278>

Academic Editors: Valentina Grumezescu and Irina Negut

Received: 3 January 2024

Revised: 19 February 2024

Accepted: 21 February 2024

Published: 25 February 2024



Copyright: © 2024 by the authors. Licensee MDPI, Basel, Switzerland. This article is an open access article distributed under the terms and conditions of the Creative Commons Attribution (CC BY) license (<https://creativecommons.org/licenses/by/4.0/>).

1. Introduction

The current market predominantly offers single-layer wound dressings, but there is growing interest in exploring the potential advantages of bilayer wound dressings [1]. Multilayer dressings present a promising alternative, allowing for the modulation of the dressing's properties [2,3].

Alginate, a biopolymer with biocompatibility and healing properties, is used in bilayer membrane design [2,3]. Commercially, it serves as a raw material for dressings under well-known brands such as Algikura-Cremer (Brazil), Kaltostat-Convatec (USA), Biatain-Coloplast (Denmark), Suprasorb-Lohmann, and Rauscher (Germany and Austria) [4].

Another extensively investigated biopolymer is chitosan, derived from the deacetylation of chitin—the second most abundant polysaccharide found in the exoskeleton of crustaceans [5]. Chitosan contributes to the design of dressings with enhanced therapeutic attributes, such as excellent oxygen permeability, control of water loss through evaporation, and promotion of drainage of exudate from lesions [5]. Chitosan's distinctive cationic character makes it a widely used component in applications involving the formation of polyelectrolyte complexes, particularly with alginate. When chitosan comes into contact with alginate, electrostatic attraction forces can form between the amino groups of chitosan (cationic) and the carboxyl groups of alginate (anionic) [6].

Studies have been conducted to explore the effectiveness of bioactive dressings containing pharmaceuticals in improving the process of wound healing [7]. Simvastatin, a statin commonly used as a hypocholesterolemic agent in cardiovascular diseases, has recently gained attention for its anti-inflammatory, anti-thrombogenic, antioxidant, and restorative effects. This pharmaceutical drug is a promising candidate for dermal treatments, especially in the context of healing wounds in diabetic patients [4,8,9].

In our previous study [10], we investigated the effects of an additional layer of alginate, whether dense or porous, on the development of alginate bilayer membranes produced through two drying methods. Furthermore, we evaluated the incorporation capacities and release rates of simvastatin through membranes with varying porosities, providing insights into the potential use of this drug for skin wound treatment. In this recent study, we created bilayer membranes using alginate and chitosan polymers loaded with simvastatin. We then evaluated the biological and physicochemical properties of the synthesized membranes, exploring the potential of bilayer membranes as a pivotal alternative for wound dressing development. These bilayer membranes can modulate drug release and enhance antimicrobial properties.

2. Materials and Methods

2.1. Materials

Membranes were produced with sodium alginate (code P.10.0057.000.00, Dinâmica, Indaiatuba, SP, Brazil), chitosan (code 448869, Sigma-Aldrich, St. Louis, MO, USA), ethanol (code 03467, Neon, São Paulo, SP, Brazil), Mueller Hinton Broth (code M1657, Himedia, Mumbai, Maharashtra, India), PBS—NaCl (code 01021, Neon, São Paulo, SP, Brazil), KCl (code P9333, Neon, São Paulo, SP, Brazil), Na₂HPO₄ (code 01395, Dinâmica, Indaiatuba, SP, Brazil); KH₂PO₄ (code P.01.0137.007.03.81, Dinâmica, Indaiatuba, SP, Brazil), glycerol (code V000123, Sigma-Aldrich, St. Louis, MO, USA) as the plasticizer, calcium chloride dihydrate (code C8103, Sigma-Aldrich, St. Louis, MO, USA) as the cross-linking agent, and simvastatin (code PHR1438, Sigma-Aldrich, St. Louis, MO, USA) as the drug to improve the wound-healing properties of the composite films. All reagents were of analytical grade and used without any further purification. *Escherichia coli* (code ATCC 11303), *Pseudomonas aeruginosa* (code ATCC 27853), and *Staphylococcus aureus* (code ATCC 25923) were obtained from the American Type Culture Collection (ATCC) (Brazil). L929 (code BCRJ 0188), and HaCat (code BCRJ 0341) were obtained from ATCC/BCRJ (Rio de Janeiro, RJ, Brazil). DMEM medium (code D5648, Sigma-Aldrich, St. Louis, MO, USA), fetal bovine serum (code 12657029, Gibco, Grand Island, NY, USA), penicillin and streptomycin (code 15140122, Gibco, Grand Island, NY, USA), sodium pyruvate (code 11360070, Gibco), and resazurin (code R7017, Sigma-Adrich, St. Louis, MO, USA) were used.

2.2. Methods

2.2.1. Preparation of Alginate Single-Layer Membranes (SLA-D)

Our current approach to producing the membranes is according to the methodology used in our previous studies [4,10]. First, 5% (*w/v*) alginate and 0.5% (*w/v*) glycerol were mixed under mechanical stirring (TE-139 stirrer, Tecnal, Piracicaba, SP, Brazil) at 600 rpm for 40 min. Then, a two-step cross-linking reaction was carried out following the method by Bierhalz et al. [11]. The in-situ cross-linking reaction began by slowly adding 40 mg

of $\text{CaCl}_2 \cdot 2\text{H}_2\text{O}$ (dissolved in 2 mL of Milli-Q water) to a 100 mL solution of alginate and glycerol. The mixture was stirred gently at 900 rpm for 30 min. Then, 25 g of this solution was transferred to a Petri dish and dried in an incubator at 40 °C for 10 h to produce a dense single-layer alginate membrane. The second step, ex-situ cross-linking, was carried out by immersing the membrane in a 4% (*w/v*) $\text{CaCl}_2 \cdot 2\text{H}_2\text{O}$ solution for 20 min. After the reaction period, the membrane was rinsed with distilled water to eliminate residual calcium ions. The membrane underwent a second drying process at 40 °C for 10 h.

2.2.2. Preparation of Alginate/Chitosan Dense Bilayer Membranes (BLAC-D)

We adapted the methodology for producing dense bilayer membranes with a chitosan bottom layer from [7]. Initially, a 2% (*w/v*) chitosan solution was dissolved in 1% (*v/v*) acetic acid. This mixture added 0.5% (*v/v*) glycerol and 5 mL of NaOH (1.0 mol/L) to adjust the pH to 5.8. This slightly acidic pH is important for keeping the skin barrier intact and protecting the skin against pathogenic microorganisms. Furthermore, the pH of injured skin (depending on the degree of complexity) tends to increase. Thus, acidic membranes tend to neutralize the region, favoring local homeostasis. Next, 25 g of chitosan solution was poured onto the alginate single-layer membrane and dried at 40 °C for 10 h. The dense bilayer membrane was cross-linked by immersion in a 4% (*w/v*) $\text{CaCl}_2 \cdot 2\text{H}_2\text{O}$ solution for 20 min. Finally, the membrane was rinsed with distilled water and dried at 40 °C for 24 h. The use of these polymers in the production of a bilayer dressing promotes electrostatic attraction forces at the points of interaction between the carboxyl groups of the alginate (anionic) and the amine groups of the chitosan (cationic), resulting in greater adhesion between the layers.

2.2.3. Preparation of Alginate/Chitosan Porous Bilayer Membranes (BLAC-P)

First, we prepared an alginate single-layer membrane as previously described. Subsequently, a 2% (*w/v*) chitosan solution in 1% (*v/v*) acetic acid was mixed with 0.5% (*v/v*) glycerol. The pH was adjusted to 5.8 using NaOH. The chitosan solution was poured onto the dried alginate single-layer membrane and frozen at −18 °C for 24 h in an ultra-freezer. After preparing the alginate/chitosan bilayer membrane, it was freeze-dried at −47 °C and 100 mmHg (L202, LIOTOP, Liobras, São Carlos, SP, Brazil) for 48 h. Then, the bilayer membrane was cross-linked by immersing it in a 4% (*w/v*) $\text{CaCl}_2 \cdot 2\text{H}_2\text{O}$ solution for 20 min. The bilayer membrane was rinsed and dried under the same conditions as before [4,10].

2.2.4. Incorporation of Simvastatin in the Single- and Bilayer Membranes (SLA-D+S, BLAC-D+S, and BLAC-P+S)

We dissolved 100 mg of simvastatin in 5 mL of ethanol and mixed it with a 5% (*w/v*) alginate solution containing 0.5% (*v/v*) glycerol until homogenization. The simvastatin concentration was the same as reported in our previous study [10], in which it was demonstrated that there is no chemical interaction between simvastatin and alginate but only physical interaction. Figure 1 illustrates the production of single- and bilayer membranes containing simvastatin.

2.2.5. Thickness

We evaluated the thickness of the membranes using the method described by Ghosal et al. [12]. The membrane thickness was calculated using a digital micrometer (Quantumike IP65, Mitutoyo, Kawasaki, Kanagawa, Japan) with 0.001 mm accuracy. The membranes were placed between the piston and the equipment support. The upper part was lowered until it touched the surface of the membrane, and the thickness was displayed on the digital screen. An average of ten measurements were recorded at random points on each of the three membranes.

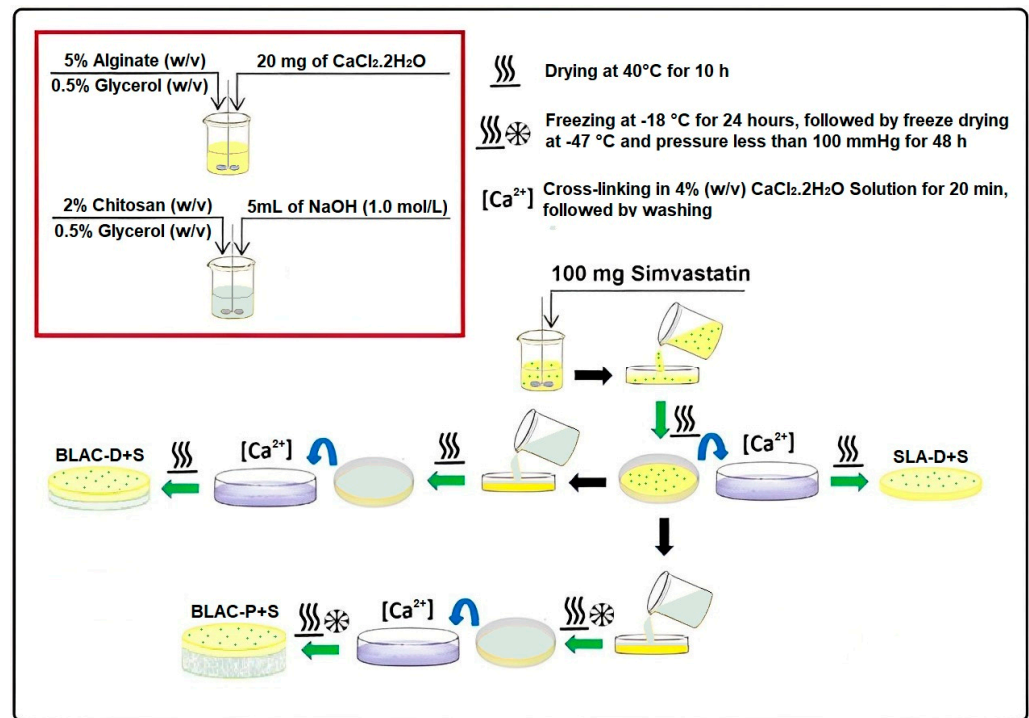


Figure 1. Flowchart of the production of the single- and bilayer membranes.

2.2.6. Swelling Study

First, we weighed the dried membrane samples ($2 \times 2 \text{ cm}^2$). Then, the membrane samples were immersed in tris(hydroxymethyl)aminomethane (TRIS) buffer (1 mol/L, pH 7) at 25 °C. The membrane samples were removed from the buffer solution at different time intervals, that is, 5, 15, and 30 min. The membranes were gently blotted with filter paper to remove surface liquid, and their weights were measured again.

$$\text{Swelling degree (\%)} = \frac{w_f - w_i}{w_f} \times 100 \quad (1)$$

where w_i is the membrane initial weight and w_f is the membrane final weight [4,10].

2.2.7. Water Vapor Permeability Rate (WVPR)

The membranes' water vapor permeability (WVP) was determined using the ASTM E96M-16 method [13]. The membrane samples were placed 5.58 mm above the water level in permeation cells containing 2 mL of deionized water. Then, the permeation cells were sealed in a desiccator and maintained under a controlled atmosphere of 37 °C and 85% relative humidity. The weight of the membranes was measured 8 times for 24 h. The water vapor permeability rate (WVPR) was calculated using the following Equation (2):

$$\text{WVPR (g/m}^2\text{h)} = \frac{w}{At} \quad (2)$$

where w is the sample weight (g), t is the time (24 h), and A is the exposed membrane area (m^2) [4,10].

2.2.8. Mechanical Properties

The mechanical properties were assessed using a universal testing machine (EMIC DL-3000, Instron, São José dos Pinhais, PR, Brazil) in tensile mode, as described in our previous study [10]. Each membrane was cut into a rectangular shape ($9 \times 80 \text{ mm}$), following ASTM D 638-99 standards [14]. The samples were vertically aligned and affixed to the clamping

claws at both ends. To maintain a constant strain rate, each sample underwent stretching at a speed of $100 \text{ mm}\cdot\text{min}^{-1}$. The tests were conducted at $25 \text{ }^\circ\text{C}$. Stress (σ) was calculated using F/A , where F represents the load force in Newtons (N) and A is the cross-sectional area measured across the width and thickness of the specimens. Deformation (ϵ) was calculated as $\Delta L/L_0$, where L_0 is the initial length and ΔL is the variation in length from the initial point. The mean and standard deviation were determined from measurements taken on ten specimens ($n = 10$).

2.2.9. Scanning Electron Microscopy (SEM)

SEM analysis was used to evaluate the morphology of the synthesized membranes. The samples were metalized with a thin layer of gold under an argon atmosphere (Polaron SC500 Sputter Coater, FISON Instruments, Ipswich, Suffolk, UK). SEM images were obtained on Quanta FEG-250 equipment (Thermo Scientific, Hillsboro, OR, USA), operating at 15 kV.

2.2.10. Infrared Spectroscopy (FTIR)

The analyses were conducted using a Cary 630 spectrophotometer (Agilent Technologies, Santa Clara, CA, USA). Spectra were acquired by ATR (attenuated total reflectance) over a wave-number range of 4000 to 650 cm^{-1} , with a resolution of 8 cm^{-1} in transmittance mode.

2.2.11. Thermal Analysis

Thermal gravimetric analysis (TGA) and differential scanning calorimetry (DSC) were employed to evaluate the thermal stability of the membranes. The experiments were conducted using a simultaneous thermal analyzer under an inert atmosphere (N_2) at a $40 \text{ mL}\cdot\text{min}^{-1}$ flow rate in an alumina ceramic crucible (NETZSCH), with a heating rate of $10 \text{ }^\circ\text{C}\cdot\text{min}^{-1}$ from $30 \text{ }^\circ\text{C}$ to $600 \text{ }^\circ\text{C}$. An empty pan was used as a reference.

2.2.12. Shelf-Life Study

The integrity and color of the membranes were evaluated for simvastatin content (Equation (2)) at $25 \pm 2 \text{ }^\circ\text{C}$ and 60% relative humidity for 15, 45, 90, and 180 days. The samples, measuring $1 \text{ cm} \times 1 \text{ cm}$, were immersed in 20 mL of TRIS buffer ($0.1 \text{ mol}\cdot\text{L}^{-1}$, pH 7) containing 20% ethanol. The simvastatin amount was determined by measuring the absorption at 238 nm using a UV/Vis spectrometer (Shimadzu, Tokyo, Japan) after stirring the samples at $37 \text{ }^\circ\text{C}$ for 96 h. The experiments were conducted in triplicate.

2.2.13. In Vitro Drug Release

The in vitro drug release was performed in Franz diffusion cells. The acceptor fluid was a TRIS buffer solution, pH 7, containing 20% ethanol. The BLCM-D+S and BLCM-P+S membranes were positioned between the donor and receptor compartments. The experiments were conducted at $37 \text{ }^\circ\text{C}$ while being stirred at 200 rpm. At predetermined time intervals (0.5, 1, 2, 4, 6, 24, 48, 72, and 96 h), 1 mL aliquots were collected and replaced with a fresh buffer solution of equal volume. The samples were analyzed for simvastatin content by UV measurements at 238 nm (U-2900, Hitachi, Tokyo, Japan). Each experiment was conducted in triplicate.

To understand how simvastatin is released, we analyzed the experimental data using two mathematical models: Higuchi (Equation (3)) and Korsmeyer-Peppas (Equation (4)). We calculated the correlation coefficients (R^2) for each model. Additionally, we used the release exponents (n) from the Korsmeyer-Peppas model to describe the release kinetics.

$$\frac{M_t}{M_\infty} = K_H t^{1/2} \quad (3)$$

$$\frac{M_t}{M_\infty} = K_P t^n \quad (4)$$

where M_t/M_∞ is the fraction of drug release, t (h) is the release time, K_H and K_P are the kinetic constants characteristic of the drug/polymer system, and n is an exponent that characterizes the drug release mechanism [15,16].

2.2.14. Antimicrobial Activity Assays

The antimicrobial activity of the chitosan layer was tested against *Escherichia coli* (ATCC 11303), *Pseudomonas aeruginosa* (ATCC 27853), and *Staphylococcus aureus* (ATCC 25923), all from the American Type Culture Collection (ATCC). These bacteria are the most common causes of skin infections [17,18]. The assay was evaluated using an indirect extract of the layer. Layer extract was prepared in 1 mL of sterile PBS, pH 7.4. The layer was maintained in the buffer solution at 37 °C for 24 h. The bacterial isolates were inoculated in 5 mL Mueller Hinton Broth (M-H Broth) and incubated at 37 °C. After 24 h, the bacterial cultures were centrifuged at 9000 rpm and 4 °C for 5 min, followed by the supernatant removal. Cells were resuspended in a fresh medium, and the inoculum was adjusted to 10^6 UFC.mL⁻¹. In a 96-well plate, 100 µL of layer extract and 100 µL of cell suspension were added to each well. The culture of bacteria in the Mueller Hinton medium was used as a control, and the Mueller Hinton medium was blank. After 18 h incubation, bacterial growth was assessed by measuring the absorbance at 620 nm (SpectraMax i3x, Molecular Device, San Jose, CA, USA). The antimicrobial activity was calculated using the following Equation (5):

$$\text{Antimicrobial activity (\%)} = \left(\frac{Abs_{sample} - Abs_{blank}}{Abs_{control}} \right) \times 100\% \quad (5)$$

2.2.15. Cytotoxicity Assays

We assessed the cytotoxicity of the membranes using the indirect method, as described in our previous study [4]. The BLCM-D+S and BLCM-P+S membranes were sterilized for ten cycles (Pulsed UV Light Emitter, SteriBeam, Gottmadingen, Germany). Sample extracts were prepared by immersing the membranes in 1 mL of supplemented Dulbecco's Modified Eagle's Medium (DMEM) containing 10% fetal bovine serum, 1% penicillin-streptomycin, and 1 mmol·L⁻¹ sodium pyruvate. Samples were kept at 5% CO₂ and 37 °C for 24 h. For the assays, mouse fibroblasts (L929) and human keratinocytes (HaCat) were seeded in DMEM medium supplemented with 10% (v/v) fetal bovine serum (FBS) and 1% (v/v) penicillin-streptomycin. In the assay, 100 µL of HaCat and L929 cells at a density of 6×10 cells/mL in supplemented DMEM were added to each well of a 96 well polystyrene plate, followed by incubation at 37 °C for 24 h. After the incubation period, the DMEM medium was replaced by 100 µL of sample extracts and incubated under the same conditions. The sample extracts were replaced by 120 µL of AlamarBlue™, 25 mg·L⁻¹ in supplemented DMEM, and metabolized for 4 h. After this period, 100 µL of metabolized medium was transferred to a 96 well plate. The fluorescence (excitation at 560 nm and emission at 590 nm) was measured on a microplate spectrophotometer, SpectraMax i3x (Molecular Devices, San Jose, CA, USA). The positive control was cells exposed to supplemented DMEM, and their viability was adjusted to 100% to calculate the mean values and standard deviation ($n = 4$). The percentage of metabolically active cells was calculated using the following Equation (6):

$$\text{Metabolically active cells (\%)} = \left(\frac{F_{sample}}{F_{positive control}} \right) \times 100\% \quad (6)$$

where F_{sample} is the fluorescence of the cells exposed to sample extracts, and $F_{positive control}$ is the fluorescence of the cells exposed to a supplemented DMEM medium.

2.2.16. Statistical Analysis

Analysis of variance (ANOVA) and the Tukey test ($\alpha = 0.05$) were employed to assess the experimental data (10.0 Statistical Software, StatSoft Inc., Tulsa, OK, USA).

3. Results and Discussion

In this research work, we produced two alginate/chitosan bilayer membranes, as indicated in Figure 1. The membranes differed from their chitosan layer. One membrane (BLAC-D) comprised two dense layers: an alginate layer as the top layer and a chitosan layer as the bottom layer. The other membrane (BLAC-P) consisted of an alginate dense layer as the top layer and a chitosan porous layer as the bottom layer. Simvastatin was added to the alginate layer, and the synthesized membranes' properties were assessed to evaluate their suitability as wound dressings.

Figure 2 shows the BLAC-D and BLAC-P membranes. As can be seen, the BLAC-D membrane had a light brown color, while the BLAC-P membrane displayed a white color. The main difference between these membranes was the morphology of the chitosan layer. This layer was translucent in the BLAC-D membrane and opaque in the BLAC-P membrane because of its porous structure. Regarding the alginate layer, both membranes displayed no visual differences.

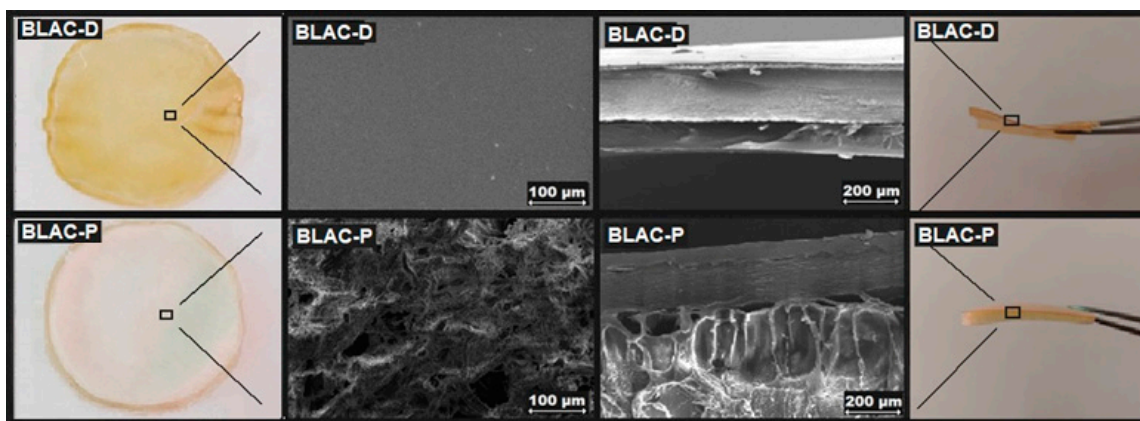


Figure 2. Images of the synthesized alginate/chitosan dense bilayer membrane (BLAC-D) and the alginate/chitosan porous bilayer membrane (BLAC-P). SEM micrographs of the dense and porous chitosan layer (on the left) and the fractures (on the right).

3.1. Thickness and Swelling Degree

Table 1 lists the thickness and swelling degree of the SLA-D, BLAC-D, and BLAC-P membranes. The thickness of the synthesized membranes was remarkably different. As expected, the SLA-D membrane displayed a small thickness. With the addition of a dense chitosan layer, BLAC-D thickness increased 1.6 times compared to SLA-D. The freeze-drying process imparted a porous structure to the chitosan layer in the BLAC-P membrane, which had a thickness 6.1 times greater than SLA-D's. A similar trend was observed for the swelling behavior, which increased as the thickness of the membranes increased. Compared to SLA-D, the swelling degree increases by 1.4 and 1.9 for BLAC-D and BLAC-P membranes, respectively. The membrane's absorption capacity was even higher in our previous study [10] with alginate bilayer membranes. The dense and porous membranes displayed an absorption capacity of approximately 1500%. This outcome was related to the carboxyl groups present in the alginate structure that strongly interact with water molecules.

Table 1. The thickness and swelling degree of the SLA-D, BLAC-D, and BLAC-P membranes.

Membranes	Thickness (mm)	Swelling Degree (%)
SLA-D	0.143 ± 0.016 ^a	414.6 ± 23.3 ^a
BLAC-D	0.222 ± 0.018 ^b	574.5 ± 23.0 ^b
BLAC-P	0.879 ± 0.030 ^c	797.3 ± 34.5 ^c

Values are indicated as the average value ± standard deviation ($n = 10$); values with similar superscript letters show a non-significant statistical difference ($\alpha = 0.05$) by the Tukey test.

3.2. WVPR and Mechanical Properties

Table 2 lists the WVPR values and the mechanical properties of the synthesized membranes. For all membranes, the WVPR values were not statistically different. Independent of the number of layers and the drying process used, the membranes had similar WVPR values. In terms of their mechanical properties, the BLAC-D membrane had a slightly higher tensile strength (σ) than the SLA-D membrane due to its greater thickness. However, the obtained values for their tensile strength were not statistically different. In contrast, the BLAC-P membrane had a lower tensile strength. The results for the maximum deformation (ϵ) showed that the BLAC-P membrane was more resistant to stress than the BLAC-D and SLA-D membranes. These findings indicated that the drying process affected the mechanical properties of the membranes; thus, it can be observed that the greater porosity in the membrane resulted in not only a greater thickness and a greater swelling degree but also lower tensile strength and maximum deformation. As indicated by the results, adding simvastatin did not affect the membrane's properties.

Table 2. The WVPR values and the mechanical properties of the membranes without (SLA-D, BLAC-D, and BLAC-P) and with simvastatin (SLA-D+S, BLAC-D+S, and BLAC-P+S).

Membranes	WVPR (g/m ² 24 h)	Tensile Strength (σ) (MPa)	Maximum Deformation (ϵ) (%)
SLA-D	2881.08 ± 160.13 ^a	22.27 ± 2.08 ^a	15.12 ± 3/00 ^a
SLA-D+S	2612.00 ± 220.67 ^a	23.27 ± 2.68 ^a	15.17 ± 2.48 ^a
BLAC-D	2650.99 ± 201.22 ^a	23.91 ± 4.61 ^a	14.51 ± 2.28 ^a
BLAC-D+S	2391.32 ± 224.57 ^a	24.03 ± 4.31 ^a	14.59 ± 2.93 ^a
BLAC-P	2893.72 ± 312.71 ^a	11.12 ± 4.63 ^b	6.70 ± 2.20 ^b
BLAC-P+S	2647.51 ± 367.23 ^a	11.90 ± 4.13 ^b	6.80 ± 2.07 ^b

Values are indicated as the average value ± standard deviation ($n = 10$); values with similar superscript letters show a non-significant statistical difference ($\alpha = 0.05$) by the Tukey test.

3.3. SEM, FTIR, and Thermal Analysis

SEM analysis was employed to evaluate the morphology of the BLAC-D and BLAC-P membranes. The micrographs of the membrane's bottom layer (chitosan layer) are shown in Figure 2. The chitosan layer of the BLAC-D membrane exhibited a smooth and dense surface, as generally observed in membranes produced by solvent evaporation [12,19]. The intersection between the alginate and chitosan layers can be observed in the fractured image of BLAC-D. In contrast, the BLAC-P membrane displayed a rough and porous surface.

Figure 3 shows the FTIR spectra of the pure compounds and the synthesized membranes. The FTIR spectrum of alginate displayed a broad band in the 3500–3200 cm⁻¹ range associated with the O-H groups' vibrations [20,21]. A small band at 2930 cm⁻¹ was attributed to saturated C-H groups [20]. The peaks at 1593 cm⁻¹ and 1418 cm⁻¹ were assigned to the asymmetric and symmetric stretching of the COO⁻ groups, respectively [20–23]. The peak at 1032 cm⁻¹ was related to the C-O-C stretching [20–22].

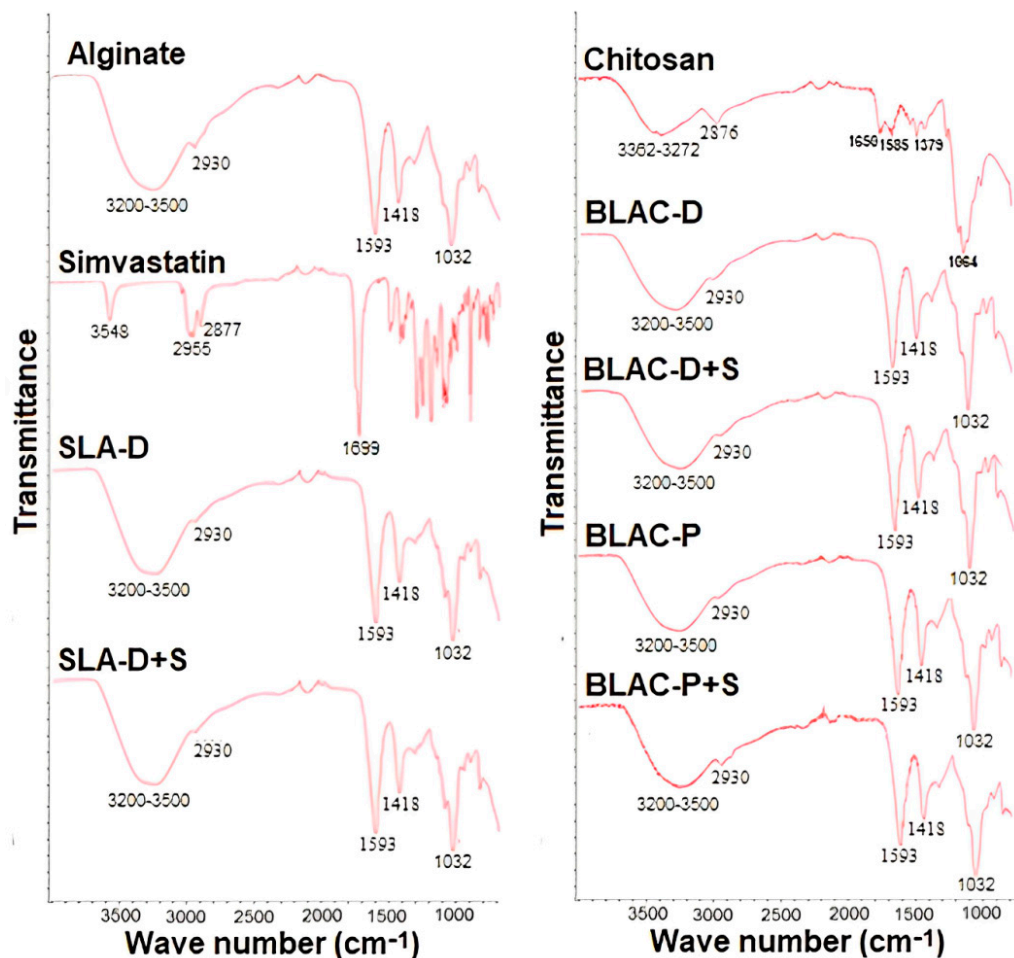


Figure 3. FTIR spectra of the pure compounds (alginate, chitosan, and simvastatin), the single- and bilayer alginate/chitosan membranes without simvastatin (SLA-D, BLAC-D, and BLAC-P), and with simvastatin (SLA-D+S, BLAC-D+S, and BLAC P+S).

The FTIR spectrum of chitosan showed a broad band in the $3362\text{--}3272\text{ cm}^{-1}$ range corresponding to the stretching of the O-H and N-H groups [24,25], while the band at 2876 cm^{-1} was associated with the C-H stretching [24,25]. The peaks at 1650 cm^{-1} and 1585 cm^{-1} were assigned to the N-H deformations [24–26]. The band at 1064 cm^{-1} was attributed to the C-O-C stretching [24–26].

The FTIR spectrum of simvastatin peaked at 3548 cm^{-1} due to the O-H groups, while the peaks at 2955 cm^{-1} and 2877 cm^{-1} were attributed to the C-H stretching. The peak at 1699 cm^{-1} was associated with the stretching vibration of the C-O and C=O carbonyl groups [27].

The FTIR spectra of the BLAC-D and BLAC-P membranes were similar to the alginate spectrum. Regarding the results, due to the greater thickness of the bilayer membranes (measured in millimeters) compared to the penetration depth allowed by the FTIR-ATR method, only the surface of the top layer of the membranes, mainly composed of alginate, could be analyzed. Consequently, no vibration bands corresponding to chitosan (found in the bottom layer) were observed. In the BLAC-D+S and BLAC-P+S spectra, there were no simvastatin characteristic peaks. This outcome could be due to simvastatin dispersion in the membrane matrix and the lack of a chemical reaction between the drug and the membrane's constituents [27].

TGA and DSC analyses evaluated the synthesized membranes' thermal properties. Regarding the SLA-D and SLA-D+S membranes, their TGA curves displayed three thermal events (Figure 4). The first event was observed in the $50\text{--}150\text{ }^{\circ}\text{C}$ temperature range and was associated with dehydration. The literature has reported that the dehydration process

involves the release of loosely attached water molecules and those strongly linked to the alginate's structure [28]. Free water molecules are released between 40 and 60 °C, while those bound to the -OH groups through dipole-dipole interaction evaporate at a higher temperature, 120 °C. The water molecules linked to the -COO⁻ groups through ion-dipole interactions are released at temperatures up to 160 °C [28]. The second thermal event was observed in the 150–350 °C temperature range and indicated a significant mass loss. This thermal event was associated with alginate degradation involving depolymerization and low-molecular-weight chain formation. The third event occurred around 350–600 °C, corresponding to the non-oxidative decomposition of the molecules generated during the alginate degradation. Simvastatin addition did not affect the degradation profile of the SLA-D membrane.

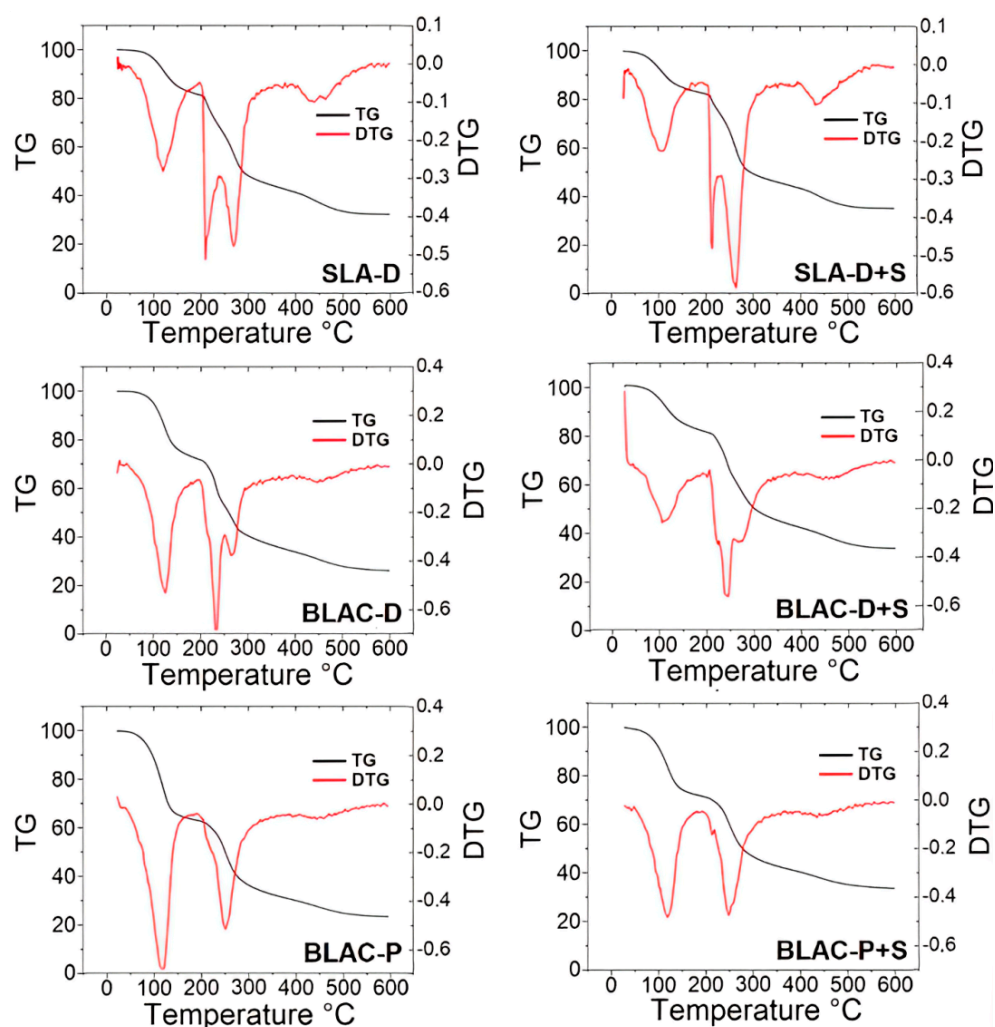


Figure 4. TGA (in black) and DTG (in red) curves of the single- and bilayer alginate/chitosan membranes without simvastatin (SLA-D, BLAC-D, and BLAC-P) and with simvastatin (SLA-D+S, BLAC-D+S, and BLAC-P+S).

The thermal curves of the BLAC-D and BLAC-P membranes exhibited two thermal events. The first event occurring at 100 °C was attributed to the dehydration process. The second one was observed at 300 °C and was related to the deacetylation and depolymerization reactions [29]. For the BLAC-D+S and BLAC-P+S membranes, the results indicated a slight increase in their residual mass, which was attributed to simvastatin degradation.

Figure 5 displays the DSC curves of the synthesized membranes. Regarding the SLA-D membrane, its DSC curve showed three peaks. The first broad endothermic peak was associated with water removal [30]. The second one at 225 °C was related to the bond

breaking, resulting in the loss of the polymeric structure. The exothermic peak in the 275–300 °C temperature range was attributed to polymer degradation [31]. The DSC curve of chitosan exhibited two peaks. The first peak was an endothermic event near 100 °C, attributed to absorbed water's evaporation [32,33]. The second peak at 300 °C corresponds to the thermal degradation of the polymeric chain, corroborating the TGA curves [32,33]. The bilayer membranes (BLAC-D, BLAC-D+S, BLAC-P, and BLAC-P+S) also presented an endothermic peak but showed a disappearance of the exothermic peak (compared to the DSC of pure chitosan), indicating that there was a loss of organization due to the formation of ionic bonds between chitosan and alginate [34]. Incorporating simvastatin into the membranes did not change the DSC curves, confirming that the drug is stable with the polymer. Furthermore, the absence of new peaks in the calorimetric curves of alginate membranes with simvastatin confirms their purity.

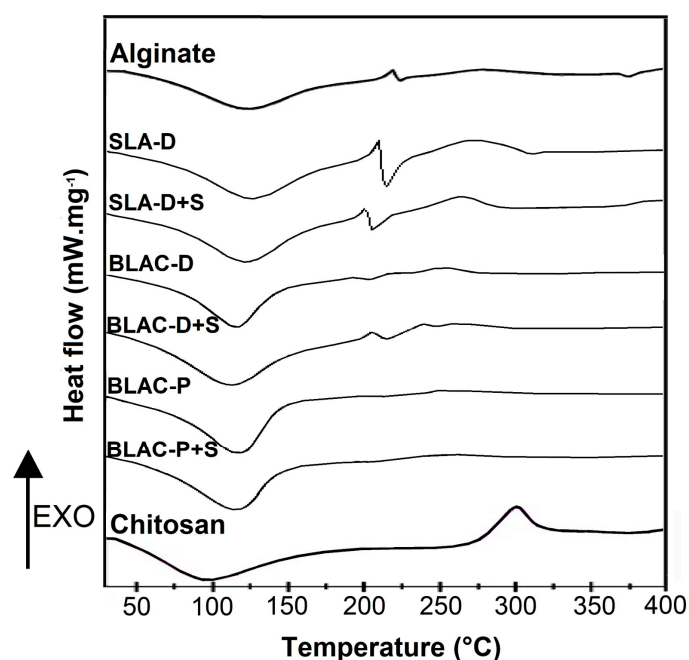


Figure 5. DSC curves of the single- and bilayer alginate/chitosan membranes without simvastatin (SLA-D, BLAC-D, and BLAC-P) and with simvastatin (SLA-D+S, BLAC-D+S, and BLAC-P+S).

3.4. Shelf-Life Study

The membranes loaded with simvastatin, BLAC-D+S and BLAC-P+S, were kept at 25 ± 2 °C and 60% relative humidity for six months. The amount of simvastatin was determined after 15, 45, 90, and 180 days (Table 3). In all membranes, 98% of simvastatin remained in the membranes after 180 days. In addition, no changes in the structure and visual appearance of the membranes were observed. The results indicated that the storage conditions were adequate to preserve the membranes and maintain their physical and chemical properties.

Table 3. Amount of simvastatin in BLAC-D+S and BLAC-P+S membranes after 15, 45, 90, and 180 days.

Time (Days)	Simvastatin (%)	
	BLAC-D+S	BLAC-P+S
15	99.9 ± 1.2	99.8 ± 2.6
45	99.7 ± 1.7	99.9 ± 2.6
90	99.6 ± 1.1	99.9 ± 2.6
180	98.9 ± 1.1	98.9 ± 1.2

3.5. In Vitro Drug Release

The release profile of simvastatin is illustrated in Figure 6. After 6 h, the SLA-D+S, BLAC-D+S, and BLAC-P+S membranes released $23.8 \pm 4.1\%$, $21.3 \pm 3.0\%$, and $23.2 \pm 3.0\%$ of simvastatin, respectively. The SLA-D+S and BLAC-P+S membranes released similar amounts of simvastatin, and this outcome could be related to the swelling behavior of the porous chitosan layer, which directly affects drug release [25], as the main mechanisms that govern drug release are degradation, swelling, and diffusion in the polymers, promoted by the differences in concentrations between media. After 96 h, the cumulative percentage was $90.3 \pm 4.1\%$ for SLA-D+S, $59.5 \pm 8.9\%$ for BLAC-D+S membrane, and $69.9 \pm 9.6\%$ for BLAC-P+S membrane. These results indicated that the use of an extra layer increased the thickness, which consequently sustained the release of simvastatin. We observed a similar trend for simvastatin release from alginate bilayer membranes [10]. In that case, the cumulative percentage was lower: $46.2 \pm 2.4\%$ for the dense membrane and $50.5 \pm 6.5\%$ for the porous membrane.

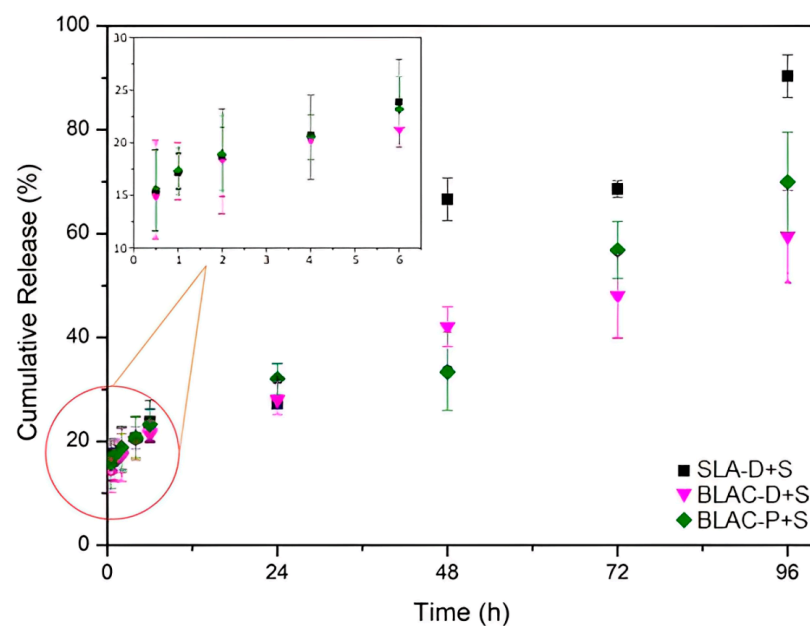


Figure 6. Release profile of simvastatin from SLA-D+S, BLAC-D+S, and BLAC-P+S membranes.

The release profile of simvastatin was fitted into the Higuchi and Korsmeyer-Peppas mathematical models. The fitting was compared based on the calculated correlation coefficients (R^2). The release kinetics of the SLA-D+S membrane fitted both models, while those of the BLAC-D+S and BLAC-P+S membranes were better fitted to the Korsmeyer-Peppas model, as indicated by the R^2 values (Table 4). Additionally, from the calculated n values (<0.5), it was possible to determine the mechanism involved in the simvastatin release. The calculated n value was <0.5 for all membranes, implying that simvastatin release followed the quasi-Fickian diffusion mechanism, in which the drug diffuses through a swollen and porous matrix [35].

Table 4. Kinetic release parameters and regression coefficients of the mathematical models.

	Higuchi		Korsmeyer-Peppas		
	K_H ($h^{-0.5}$)	R^2	K_P ($\mu g/h^{-n}$)	n	R^2
SLA-D+S	0.084	0.93	0.148	0.36	0.95
BLAC-D+S	0.066	0.53	0.133	0.28	0.90
BLAC-P+S	0.072	0.47	0.150	0.27	0.84

3.6. Antimicrobial Activity Assays

Chitosan, present in the lower layer of bilayer membranes, has been used as an antibacterial agent by several authors because of the interaction between chitosan (positively charged) and the cell walls of bacteria (negatively charged), resulting in the interruption of bacterial activity [36]. It is very important in the treatment of wounds that show signs of inflammation caused by bacterial infection to have a faster release of the drug with an anti-inflammatory effect in the first hours and to have greater absorption, as these wounds may appear with yellowish secretion, a lousy smell, worsening of pain, redness, or swelling. As BLAC-P+S demonstrated faster release and greater absorption, the antimicrobial activity test was carried out on its lower layer. As indicated in Figure 7, the result of the antimicrobial activity assay demonstrated growth inhibitions for the bacteria *Pseudomonas aeruginosa* (ATCC 27853), *Escherichia coli* (ATCC 11303), and *Staphylococcus aureus* (ATCC 25923) of 100.00 ± 0.60 , 100.00 ± 0.44 , and $99.99 \pm 0.25\%$, respectively. The test was also performed on commercial alginate, resulting in growth inhibitions of 0.00 ± 3.73 , 27.00 ± 9.99 , and $0.00 \pm 1.90\%$, respectively. To have a significant antibacterial action, an action above 70% is desirable [17,18], so the alginate did not show an antibacterial effect, proving that the entire effect is related only to the chitosan layer.

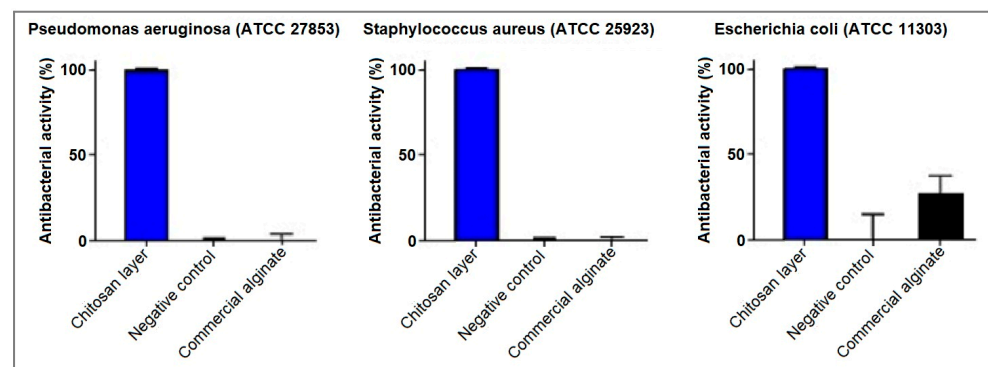


Figure 7. Antimicrobial activity assay of the chitosan layer of the BLAC-P+S membrane.

Promising results of antibacterial activity were also described by Kiti and Suwanton (2020) [7], who separately studied the activity of the chitosan layer of a bilayer membrane. The results showed a percentage reduction of 84.10 and 88.79% in the activity of *Escherichia coli* and *Staphylococcus aureus*, respectively. Another way to study the antibacterial effect of chitosan was reported by Pasaribu et al. (2023) [36], who periodically placed the chitosan-containing dressing on rat wounds for microbiological examination. From the results, they concluded that the chitosan content in the sample had antibacterial properties that played a role in preventing the growth of bacteria, as the rats treated with the samples had lower amounts of bacteria in the wounds. Another recent study of the antibacterial effect of chitosan was reported by Mone et al. (2023) [37], in which, from the results, they concluded that the chitosan content in the sample had antibacterial properties that played a role in preventing the growth of bacteria, as the rats treated with the samples had lower amounts of bacteria in the wounds. Therefore, BLAC-P+S proved to be ideal for treating infected wounds.

3.7. Cytotoxicity Assays

The cytotoxicity assays evaluated the potential harmful effects of the synthesized membranes on the keratinocytes (predominant cells in the epidermis) and fibroblasts (main cells in the dermis) (Figure 8). Each cell lineage represents one of the skin's structures. Therefore, cell viability results represent responses to wounds that are superficial as well as deep. The SLA-D membrane displayed similar cytotoxic effects for both cells. On the other hand, the bilayer membranes affected the cells differently. The BLAC-D membrane was more cytotoxic to the keratinocytes than to the fibroblasts. The BLAC-P membrane

showed comparable outcomes. It is worth noting that the bilayer membranes had a higher cytotoxic effect than the single-layer membrane. In our previous study [10], we observed a similar trend with single- and bilayer alginate membranes. The cytotoxic effects on the keratinocyte cells were higher for the bilayer membranes, which were dense ($80.7\% \pm 5.4$) and porous ($78.2\% \pm 6.0$), than for the single-layer membrane ($104.6\% \pm 7.9$).

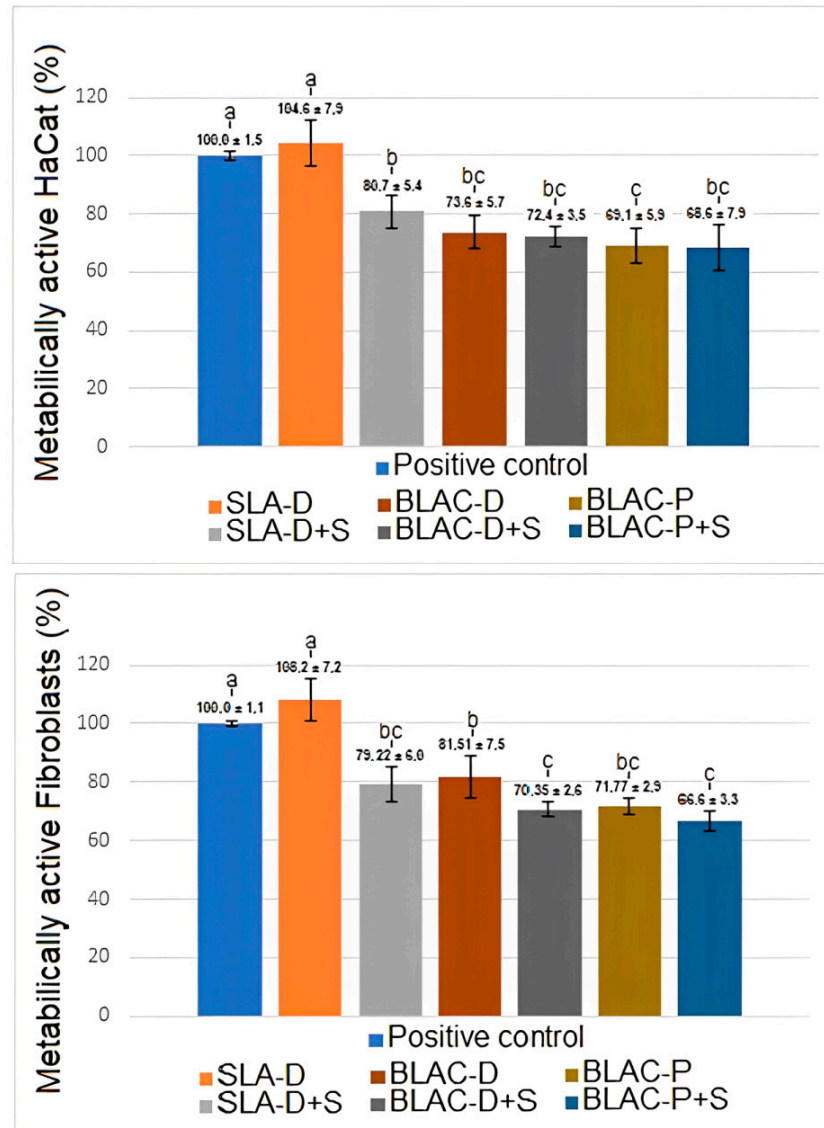


Figure 8. Indirect cytotoxicity of single- and bilayer membranes without simvastatin (SLA-D, BLAC-D, and BLAC-P) and with simvastatin (SLA-D+S, BLAC-D+S, and BLAC-P+S).

Regarding the cytotoxicity of the membranes containing simvastatin, the SLA D+S, BLAC-D+S, and BLAC-P+S membranes showed non-significant statistical differences. The results indicated that simvastatin addition affected cell viability. These findings could be due to the simvastatin hydrophobicity, which enables the drug to penetrate the cell membranes. Once inside the cells, simvastatin could affect the cell biochemistry and induce cell death [37]. Kupcsik et al. [38] investigated the effect of simvastatin on human mesenchymal stem cells. The authors observed that cell viability was dependent on simvastatin concentration. At low concentrations ($<1 \mu\text{M}$), simvastatin did not significantly affect cell viability. In contrast, exposure to high concentrations ($5 \mu\text{M}$) resulted in a significant drop in cell viability after a few days. The study found that prolonged exposure to high levels of simvastatin harmed cell viability. According to ISO 10993-5 guidelines [39],

the produced material must present a minimum of 70% cell viability. Therefore, SLA-D+S, BLAC-D+S, and BLAC-P+S membranes are suitable for the proposed application. Due to the cytocompatibility profile of these membranes, in addition to their potential application as a dressing, the membranes can also be used as a device for digital toxicology tests, being able to monitor the physiological conditions (pH, necrotic tissue, infection, exudate, and bleeding) of the wound [40].

4. Conclusions

In summary, the comprehensive physicochemical analysis of the alginate/chitosan bilayer membranes underscored their suitability for wound dressing applications. The BLAC-D and BLAC-P membranes exhibited distinct characteristics regarding swelling behavior and mechanical properties despite sharing closely aligned water vapor permeability rates (WVPR). The sustained release of simvastatin over 96 h from both BLAC-D and BLAC-P membranes added another dimension to their potential therapeutic utility. Furthermore, cytotoxicity assays affirmed that both membrane types, BLAC-D and BLAC-P, meet the requirements for practical wound dressing applications, highlighting the use of BLAC-P+S in treating infected wounds. This collective evidence positions these bilayer membranes as promising candidates in wound care.

Author Contributions: Conceptualization, R.S.V. and N.F.V.; methodology, R.S.V. and R.T.M.; validation, F.K.A.; formal analysis, R.T.M., T.F.D.S. and A.L.B.S.; investigation, R.T.M., T.F.D.S. and R.N.F.M.F.; resources, R.S.V.; data curation, R.T.M. and R.N.F.M.F.; writing—original draft preparation, R.T.M. and L.d.S.G.; writing—review and editing, R.S.V., N.F.V. and L.d.S.G.; visualization, R.T.M.; supervision, R.S.V. and N.F.V.; project administration, R.S.V.; funding acquisition, R.S.V. All authors have read and agreed to the published version of the manuscript.

Funding: This research was funded by CAPES (Coordenação de Aperfeiçoamento de Pessoal de Nível Superior) (grant number: 877770-4/4110.1/1/,/0) and CNPq (Conselho Nacional de Desenvolvimento Científico e Tecnológico) (grant number: 442734/2020-4).

Institutional Review Board Statement: Not applicable.

Informed Consent Statement: Not applicable.

Data Availability Statement: Data are contained within the article.

Acknowledgments: The authors acknowledge the Brazilian funding agencies CAPES (Coordenação de Aperfeiçoamento de Pessoal de Nível Superior), CNPq (Conselho Nacional de Desenvolvimento Científico e Tecnológico), and Central Analítica—UFC (funded by FINEP-CT-INFRA, CAPES-Pró-Equipamentos, and MCTI-CNPq-SisNano 2.0) for their support in the SEM analyses.

Conflicts of Interest: The authors declare no conflicts of interest.

References

1. Wang, L.; Wang, W.; Liao, J.; Wang, F.; Jiang, J.; Cao, C.; Li, S. Novel bilayer wound dressing composed of SIS membrane with SIS cryogel enhanced wound healing process. *Mater. Sci. Eng. C Mater. Biol. Appl.* **2018**, *85*, 162–169. [[CrossRef](#)] [[PubMed](#)]
2. Thu, H.-E.; Zulfakar, M.H.; Ng, S.-F. Alginate based bilayer hydrocolloid films as potential slow-release modern wound dressing. *Int. J. Pharm.* **2012**, *434*, 375–383. [[CrossRef](#)] [[PubMed](#)]
3. Maver, T.; Gradišnik, L.; Kurečić, M.; Hribernik, S.; Smrke, D.M.; Maver, U.; Kleinschek, K.S. Layering of different materials to achieve optimal conditions for treatment of painful wounds. *Int. J. Pharm.* **2017**, *529*, 576–588. [[CrossRef](#)] [[PubMed](#)]
4. Monteiro, R.T.; Andrade, F.K.; Vasconcelos, N.F.; Nogueira, K.A.B.; Petrilli, R.; Vieira, R.S. Production and characterization of alginate bilayer membranes for releasing simvastatin to treat wounds. *Biointerphases* **2020**, *15*, 041002. [[CrossRef](#)] [[PubMed](#)]
5. Mi, F.-L.; Shyu, S.-S.; Wu, Y.-B.; Lee, S.-T.; Shyong, J.-Y.; Huang, R.-N. Fabrication and characterization of a sponge-like asymmetric chitosan membrane as a wound dressing. *Biomaterials* **2001**, *22*, 165–173. [[CrossRef](#)]
6. Bakshi, P.S.; Selvakumar, D.; Kadirvelu, K.; Kumar, N.S. Chitosan as an environment friendly biomaterial—A review on recent modifications and applications. *Int. J. Biol. Macromol.* **2020**, *150*, 1072–1083. [[CrossRef](#)]
7. Kiti, K.; Suwanton, O. Bilayer wound dressing based on sodium alginate incorporated with curcumin- β -cyclodextrin inclusion complex/chitosan hydrogel. *Int. J. Biol. Macromol.* **2020**, *164*, 4113–4124. [[CrossRef](#)]
8. Al-Ghoul, W.M.; Kim, M.S.; Fazal, N.; Azim, A.C.; Ali, A. Evidence for simvastatin anti-inflammatory actions based on quantitative analyses of NETosis and other inflammation/oxidation markers. *Results Immunol.* **2014**, *4*, 14–22. [[CrossRef](#)]

9. Yarasvini, S.; Anusa, R.S.; VedhaHari, B.N.; Prabhu, P.C.; RamyaDevi, D. Topical hydrogel matrix loaded with Simvastatin microparticles for enhanced wound healing activity. *Mater. Sci. Eng. C Mater. Biol. Appl.* **2017**, *72*, 160–167. [[CrossRef](#)] [[PubMed](#)]
10. Monteiro, R.T.; Da Silva, T.F.; Filho, R.N.F.M.; Vasconcelos, N.F.; Nogueira, K.A.B.; Petrilli, R.; Andrade, F.K.; Vieira, R.S. Simvastatin-loaded alginate bilayer membranes for wound dressing applications. *J. Drug Deliv. Sci. Technol.* **2023**, *86*, 104701. [[CrossRef](#)]
11. Bierhalz, A.C.K.; da Silva, M.A.; de Sousa, H.C.; Braga, M.E.M.; Kieckbusch, T.G. Influence of natamycin loading methods on the physical characteristics of alginate active films. *J. Superfruit. Fluids* **2013**, *76*, 74–82. [[CrossRef](#)]
12. Ghosal, K.; Das, A.; Das, S.K.; Mahmood, S.; Ramadan, M.A.M.; Thomas, S. Synthesis and characterization of interpenetrating polymeric networks based bio-composite alginate film: A well-designed drug delivery platform. *Int. J. Biol. Macromol.* **2019**, *130*, 645–654. [[CrossRef](#)] [[PubMed](#)]
13. *ASTM E96/E96M-16*; Standard Test Methods for Water Vapor Transmission of Materials. ASTM: West Conshohocken, PA, USA, 2016. [[CrossRef](#)]
14. *ASTM D638-99*; Standard Test Method for Tensile Properties of Plastics. ASTM: West Conshohocken, PA, USA, 1999. [[CrossRef](#)]
15. Korsmeyer, R.W.; Gurny, R.; Doelker, E.; Buri, P.; Peppas, N.A. Mechanisms of solute release from porous hydrophilic polymers. *Int. J. Pharm.* **1983**, *15*, 25–35. [[CrossRef](#)]
16. Sikareepaisan, P.; Ruktanonchai, U.; Supaphol, P. Preparation and characterization of asiaticoside-loaded alginate films and their potential for use as effectual wound dressings. *Carbohydr. Polym.* **2011**, *83*, 1457–1469. [[CrossRef](#)]
17. Glik, J.; Kawecki, M.; Gaździk, T.; Nowak, M. The impact of the types of microorganisms isolated from blood and wounds on the results of treatment in burn patients with sepsis. *Pol. Przegl. Chir.* **2012**, *84*, 6–16. [[CrossRef](#)]
18. Puca, V.; Marulli, R.Z.; Grande, R.; Vitale, I.; Niro, A.; Molinaro, G.; Prezioso, S.; Muraro, R.; Di Giovanni, P. Microbial species isolated from infected wounds and antimicrobial resistance analysis: Data emerging from a three-years retrospective study. *Antibiotics* **2021**, *10*, 1162. [[CrossRef](#)] [[PubMed](#)]
19. Thu, H.-E.; Ng, S.-F. Gelatine enhances drug dispersion in alginate bilayer film via the formation of crystalline microaggregates. *Int. J. Pharm.* **2013**, *454*, 99–106. [[CrossRef](#)]
20. Ren, H.; Gao, Z.; Wu, D.; Jiang, J.; Sun, Y.; Luo, C. Efficient Pb(II) removal using sodium alginate–carboxymethyl cellulose gel beads: Preparation, characterization, and adsorption mechanism. *Carbohydr. Polym.* **2016**, *137*, 402–409. [[CrossRef](#)]
21. Kuila, S.B.; Ray, S.K. Separation of benzene–cyclohexane mixtures by filled blend membranes of carboxymethyl cellulose and sodium alginate. *Sep. Purif. Technol.* **2014**, *123*, 45–52. [[CrossRef](#)]
22. Li, Y.; Jia, H.; Pan, F.; Jiang, Z.; Cheng, Q. Enhanced anti-swelling property and dehumidification performance by sodium alginate–poly(vinyl alcohol)/polysulfone composite hollow fiber membranes. *J. Membr. Sci.* **2012**, *407–408*, 211–220. [[CrossRef](#)]
23. Dong, Z.; Wang, Q.; Du, Y. Alginate/gelatin blend films and their properties for drug controlled release. *J. Membr. Sci.* **2006**, *280*, 37–44. [[CrossRef](#)]
24. Mukhopadhyay, P.; Sarkar, K.; Soam, S.; Kundu, P.P. Formulation of pH-responsive carboxymethyl chitosan and alginate beads for the oral delivery of insulin. *J. Appl. Polym. Sci.* **2013**, *129*, 835–845. [[CrossRef](#)]
25. Di Martino, A.; Kucharczyk, P.; Capakova, Z.; Humpolicek, P.; Sedlarik, V. Chitosan-based nanocomplexes for simultaneous loading, burst reduction and controlled release of doxorubicin and 5-fluorouracil. *Int. J. Biol. Macromol.* **2017**, *102*, 613–624. [[CrossRef](#)]
26. Kim, S.-G.; Lim, G.-T.; Jegal, J.; Lee, K.-H. Pervaporation separation of MTBE (methyl tert-butyl ether) and methanol mixtures through polyion complex composite membranes consisting of sodium alginate/chitosan. *J. Membr. Sci.* **2000**, *174*, 1–15. [[CrossRef](#)]
27. Rezvanian, M.; Amin, M.C.I.M.; Ng, S.-F. Development and physicochemical characterization of alginate composite film loaded with simvastatin as a potential wound dressing. *Carbohydr. Polym.* **2016**, *137*, 295–304. [[CrossRef](#)] [[PubMed](#)]
28. Avella, M.; Pace, E.D.; Immirzi, B.; Impallomeni, G.; Malinconico, M.; Santagata, G. Addition of glycerol plasticizer to seaweeds derived alginates: Influence of microstructure on chemical–physical properties. *Carbohydr. Polym.* **2007**, *69*, 503–511. [[CrossRef](#)]
29. de Britto, D.; Campana-Filho, S.P. Kinetics of the thermal degradation of chitosan. *Thermochim. Acta* **2007**, *465*, 73–82. [[CrossRef](#)]
30. Russo, R.; Malinconico, M.; Santagata, G. Effect of cross-linking with calcium ions on the physical properties of alginate films. *Biomacromolecules* **2007**, *8*, 3193–3197. [[CrossRef](#)] [[PubMed](#)]
31. Pereira, R.; Carvalho, A.; Vaz, D.C.; Gil, M.H.; Mendes, A.; Bártolo, P. Development of novel alginate based hydrogel films for wound healing applications. *Int. J. Biol. Macromol.* **2013**, *52*, 221–230. [[CrossRef](#)] [[PubMed](#)]
32. Guinesi, L.S.; Cavalheiro, É.T.G. The use of DSC curves to determine the acetylation degree of chitin/chitosan samples. *Thermochim. Acta* **2006**, *444*, 128–133. [[CrossRef](#)]
33. López, F.A.; Mercê, A.L.R.; Alguacil, F.J.; López-Delgado, A. A kinetic study on the thermal behaviour of chitosan. *J. Therm. Anal. Calorim.* **2008**, *91*, 633–639. [[CrossRef](#)]
34. Abruzzo, A.; Bigucci, F.; Cerchiara, T.; Saladini, B.; Gallucci, M.C.; Cruciani, F.; Vitali, B.; Luppi, B. Chitosan/alginate complexes for vaginal delivery of chlorhexidine digluconate. *Carbohydr. Polym.* **2013**, *91*, 651–658. [[CrossRef](#)] [[PubMed](#)]
35. Suratman, A.; Purwaningsih, D.R.; Kunarti, E.S.; Kuncaka, A. Controlled release fertilizer encapsulated by glutaraldehyde-crosslinked chitosan using freeze-drying method. *Indones. J. Chem.* **2020**, *20*, 1414–1421. [[CrossRef](#)]
36. Pasaribu, K.M.; Ilyas, S.; Tamrin, T.; Radecka, I.; Swingler, S.; Gupta, A.; Stamboulis, A.G.; Gea, S. Bioactive bacterial cellulose wound dressings for burns with collagen in-situ and chitosan ex-situ impregnation. *Int. J. Biol. Macromol.* **2023**, *230*, 123118. [[CrossRef](#)] [[PubMed](#)]

37. Mone, N.S.; Syed, S.; Ravichandiran, P.; Kamble, E.E.; Pardesi, K.R.; Salunke-Gawali, S.; Rai, M.; Singh, A.V.; Dakua, S.P.; Park, B.H.; et al. Synergistic and Additive Effects of Menadione in Combination with Antibiotics on Multidrug-Resistant *Staphylococcus aureus*: Insights from Structure-Function Analysis of Naphthoquinones. *ChemMedChem* **2023**, *18*, 24. [[CrossRef](#)]
38. Kupcsik, L.; Meurya, T.; Flury, M.; Stoddart, M.; Alini, M. Statin-induced calcification in human mesenchymal stem cells is cell death related. *J. Cell. Mol. Med.* **2009**, *13*, 4465–4473. [[CrossRef](#)]
39. *ISO 10993-5:2009*; Biological Evaluation of Medical Devices. Part 5: Tests for In Vitro Cytotoxicity. ISO: Geneva, Switzerland, 2009.
40. Singh, A.V.; Bansod, G.; Mahajan, M.; Dietrich, P.; Singh, S.P.; Rav, K.; Thissen, A.; Bharde, A.M.; Rothenstein, D.; Kulkarni, S.; et al. Digital Transformation in Toxicology: Improving Communication and Efficiency in Risk Assessment. *ACS Omega* **2023**, *24*, 21377–21390. [[CrossRef](#)]

Disclaimer/Publisher’s Note: The statements, opinions and data contained in all publications are solely those of the individual author(s) and contributor(s) and not of MDPI and/or the editor(s). MDPI and/or the editor(s) disclaim responsibility for any injury to people or property resulting from any ideas, methods, instructions or products referred to in the content.